

Electronic Supplementary Information (ESI) for

Defective 1T-VS₂ with Fibonacci Pattern Unlocking High Mass-Loading and Self-Charging Cathodes for Aqueous Zinc-Ion Batteries

Tao Li^a, Xinji Dong^a, Hange Yang^a, Jianwei Zhang^b, Rong Huang^b, Zhuoran Lv^a, Yueyue Li^a, Shicong Zhang^a, Fuqiang Huang^{*a} and Tianquan Lin^{*a}

¹ School of Materials Science and Engineering, Zhangjiang Institute for Advanced Study (ZIAS), Shanghai Jiao Tong University, Shanghai, PR China;

² Key Laboratory of Polar Materials and Devices (MOE), Department of Electronics, East China Normal University, Shanghai 200241, China.

Experimental section

Preparation of the Rose D-VS₂

The Rose D-VS₂ material was synthesized through a hydrothermal reaction followed by thermal treatment. Specially, 2 mmol NH₄VO₃ (99.95% purity, Macklin) was added to a mix solvent consisting of 10 mL of H₂O and 20 mL of ethylene glycol (99.5% purity, Macklin), resulting in a clear solution after magnetic stirring. Subsequently, 18 mmol thioacetamide (99% purity, Macklin) was introduced to above solution. After stirring for 30 minutes, 1.5 mL ammonia (28%, Macklin) was added dropwise to the mixture. Following another 1 hour of stirring, the solution was transferred to a 50 mL Teflon-lined stainless autoclave and heated at 180°C. The heating duration was set for 5 hours to achieve VS₂ nanoparticles and extended to 48 hours for the formation of rose-like morphology. After cooling to the room temperature, specific VS₂ materials were obtained by vacuum filtration with deionized water and ethanol for three times and vacuum drying at 60 °C for 24 hours. To enable the self-intercalation of V atoms, the rose VS₂ material underwent heating in a tube furnace at 300 °C for 3 hours under an H₂/Ar flow (10% H₂) at a rate of 80 sccm min⁻¹. Finally, black Rose D-VS₂ powders are obtained.

Electrochemical measurements

The VS₂ cathode was fabricated utilizing dry coating technology. The active materials were mixed with Ketjin black and polytetrafluoroethylene in a weight ratio of 8:1:1 to produce a self-supporting film. This film was subsequently pressed onto the titanium mesh (100 mesh) to form the final cathode. In accordance with the specified testing requirements, the mass loading range of 10 - 30 mg cm⁻² can be achieved through regulating the thickness of the self-supporting film. Cyclic voltammogram (CV) curves were measured on an electrochemical workstation (CHI670E). The electrochemical performance of the coin cell was assessed utilizing CR2016 coin-type cells on a NEWARE battery test system (MIHW-200-160CH-B, Shenzhen, China) at a constant temperature of 25 °C. The zinc foil (>99.99% purity, Guangdong Canrd New Energy Technology Co. Ltd.) and glass fiber (Whatman GF/D) was employed as the anode and the separator, respectively. The electrolyte utilized is 2 M Zn(OTf)₂ (98% purity,

Aladdin) aqueous solution. The amount of electrolyte injected per coin cell is 50 μL . EIS measurements were conducted on different VS_2 cathodes with the mass loading of 10 mg cm^{-2} with the frequency range from 0.01 Hz to 10^6 Hz.

Materials characterization

The chemical configurations of samples were investigated by XPS (Thermo Fisher Scientific Nexsa instrument) and EPR spectra (ESR500). The crystal structure of all materials was identified based-on XRD patterns using a Bruker D8 ADVANCE instrument with $\text{Cu-K}\alpha$ (1.5406 \AA) irradiation at room temperature. The macro-morphology of all VS_2 materials was characterized by SEM (Apreo 2C) with an electron beam energy of 10 kV. The cross-section morphology was obtained by SEM-FIB (GAIA3). Nitrogen adsorption/desorption isotherms were obtained employing an ASAP2460 analyser. The atomic structure of the Rose V- VS_2 material was analysed by ACTEM (Spectra 300, ThermoFisher Scientific). The contact angle measurements were conducted utilizing a contact angle measuring instrument (DSA100). The elemental compositions of samples were ascertained by ICP-MS (NexION5000G). The XAFS of S K -edge was performed on the soft X-ray spectroscopy beamline at Shanghai Synchrotron Radiation Facility. The electric conductivity was conducted by using the standard four-probe method on a Quantum Design Physical Property Measurement System (PPMS).

Calculation

COMSOL calculation

The modelling of the ion accumulation-diffusion process was performed in COMSOL Multiphysics software with diluted species transport module and electrical module. By employing the tertiary current distribution and concentration diffusion equations to monitor both current and concentration distributions, the flux of each ion in the electrolyte can be determined through the application of the Nernst-Planck equation.

$$N_i = -D_i \left(\nabla c_i + \frac{F}{RT} z_i c_i \nabla \phi_l \right), i = 1, 2, \dots, n$$

Where D_i , N_i , c_i , z_i , F , T , R , and ϕ_l denote the diffusion coefficient, the flux, the concentration, the charge number, the Faradaic constant, temperature, gas constant, and

electrolyte potential, respectively. l stands for the position along the diffusion region of thickness d ($0 < l < d$).

The assumption of electroneutrality is represented as follows:

$$F \sum_{i=1}^n z_i c_i = 0$$

Based on the steady-state continuity equations and the law of mass conservation, we derive:

$$\frac{\partial c_i}{\partial t} + \nabla \cdot N_i = 0$$

The boundary condition is established as follows:

$$\vec{n} \cdot J = 0$$

where J means the species flux on the boundary face.

The governing equations for electrochemical reactions and concentration distribution are outlined below. It is evident that electrochemical reactions serve as source terms, supplying reactants to the diffusion equation. The reaction rate adheres to the Arrhenius equation:

$$R = A e^{-E_a/RT}$$

In the equation, c represents the concentration, J represents the flux of diffusion, R is the reaction rate, k is the rate constant; A is the characteristic constant of the given reaction, known as the pre-exponential factor; e is the base of natural logarithm (2.718); R is the gas constant ($8.314 \text{ J} \cdot \text{mol}^{-1} \cdot \text{K}^{-1}$), E_a is the activation energy of the reaction.

Therefore, the concentration equation can be rewritten as:

$$\frac{\partial c_i}{\partial t} + \nabla \cdot J_i + u \cdot \nabla c_i = R_i$$

Due to variations in shape and surface reaction coefficients between the two materials, distinct reactant concentrations can be achieved.

Within the bulk domain, a uniform concentration was assumed to equal to the bulk concentration, where the products have the initial concentration of 2000 mol m^{-3} . An electric potential of 0 V is applied across the outer surface of this bulk domain.

Additionally, ions are generated from the electrode's surface.

Density functional theory simulation

The first-principle-based geometry optimization calculations were carried out within density-functional theory (DFT), implemented in the Vienna Ab Initio Simulation Package (VASP) code¹, using the frozen-core projector augmented-wave (PAW) method to describe the interaction between the atomic cores and the valence electron density.² The exchange-correlation potential was approximated within the generalized gradient approximation (GGA) using the Perdew-Burke Ernzerhof (PBE) functional.³ The dispersion corrected DFT-D3 schemes was employed to describe the Van der Waals (vdW) interactions.⁴ Plane-wave cutoff energy was set to 450 eV. The conjugate gradient algorithm was used in ionic optimization, convergence threshold was set to 10^{-5} eV atom⁻¹ in electronic relaxation and 0.05 eV Å⁻¹ in Hellmann–Feynman force on each atom. The Brillouin zone in reciprocal space was sampled by a Γ -centered Monkhorst–Pack scheme with $3 \times 3 \times 1$ for geometry optimization and electronic structure calculations.

DRT analysis

Distribution relaxation times (DRT) from the EIS data were calculated using MatlabR2023b with a toolbox of DRT-TOOLS developed by Professor Francesco Ciucci's research group. The DRT-TOOLS can be freely accessed at the following site: <https://github.com/ciuccislab>.

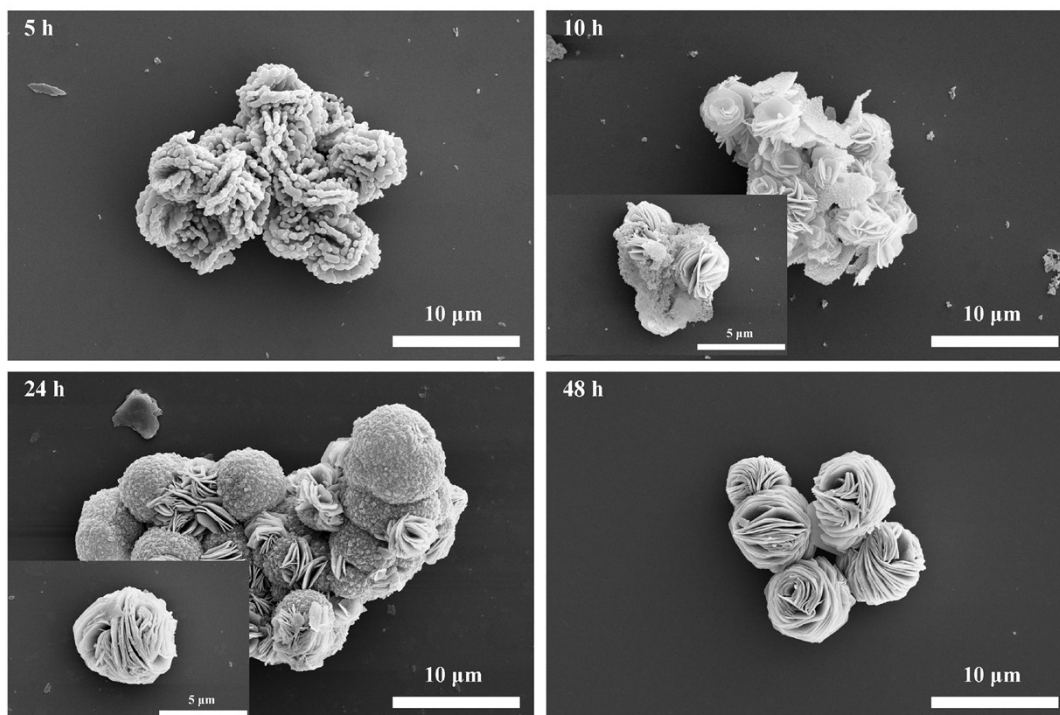


Fig. S1 SEM images showing the morphological evolution of the Rose D-VS₂.

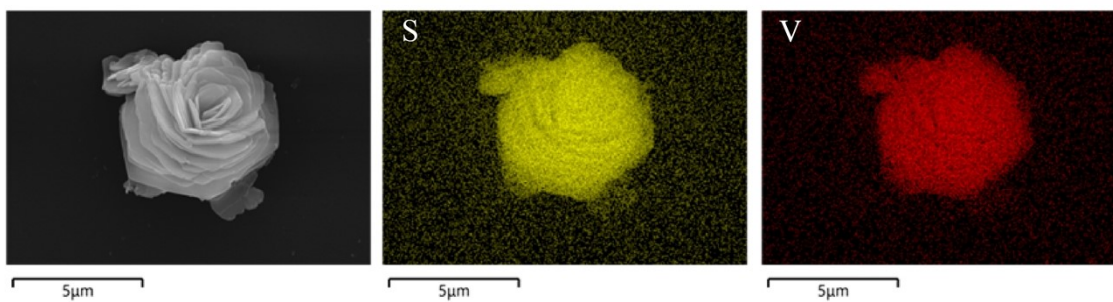


Fig. S2 SEM image and corresponding energy-dispersive X-ray spectroscopy (EDS) mapping showing the micro-rose structure of the Rose D-VS₂.

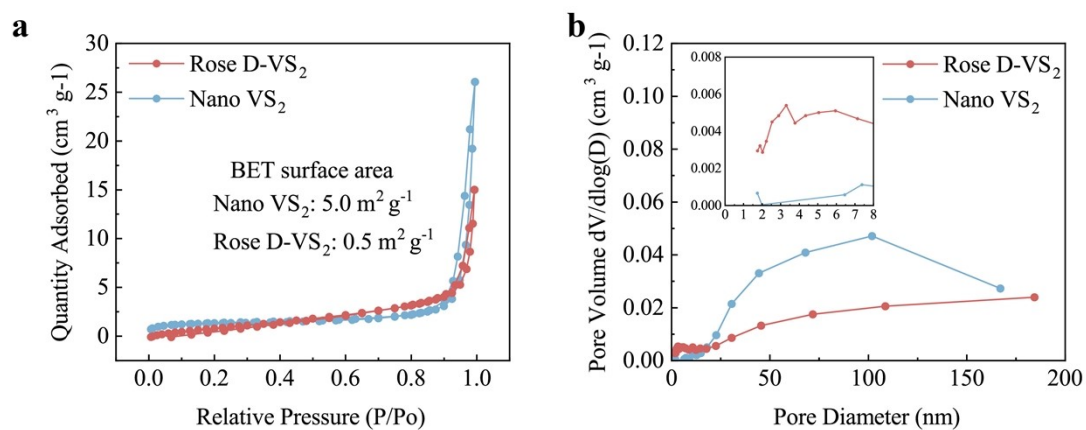


Fig. S3 The specific surface area and pore size distribution of various VS_2 materials. a) Nitrogen adsorption and desorption isotherms. b) Pore size distribution.

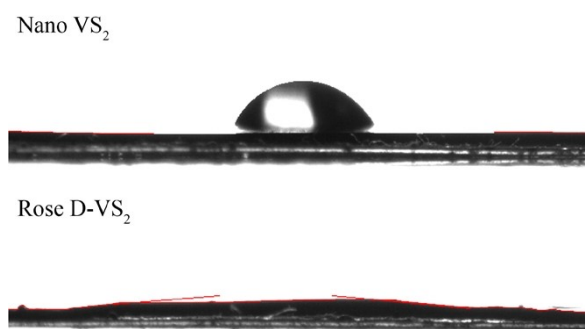


Fig. S4 Contact angles of various VS_2 materials in relation to electrolytes.

Despite showing a relatively small specific surface area, the Rose D- VS_2 exhibits superior electrolyte wettability compared to the Nano VS_2 .

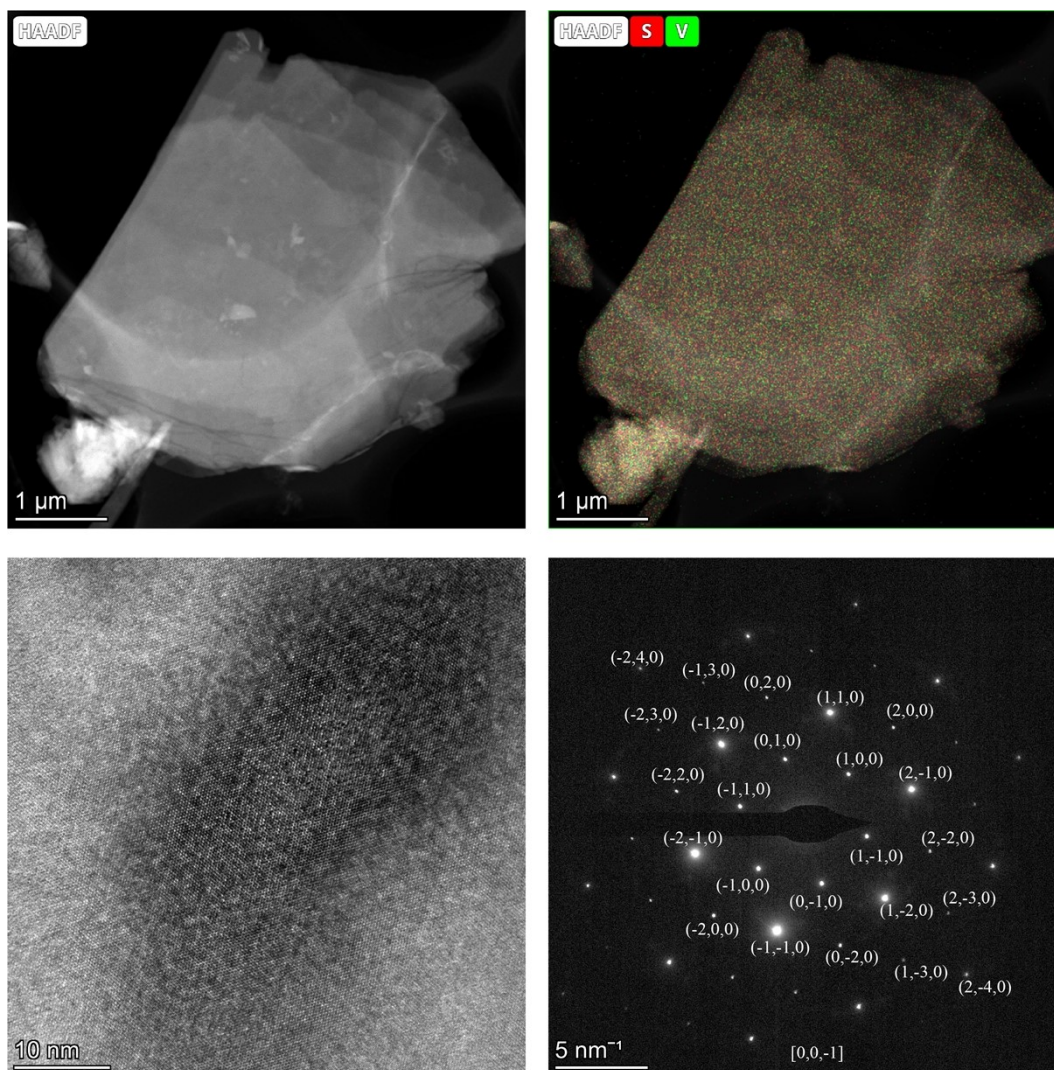


Fig. S5 TEM images, EDS mapping, and corresponding selected area electron diffraction pattern of the Rose D-VS₂.

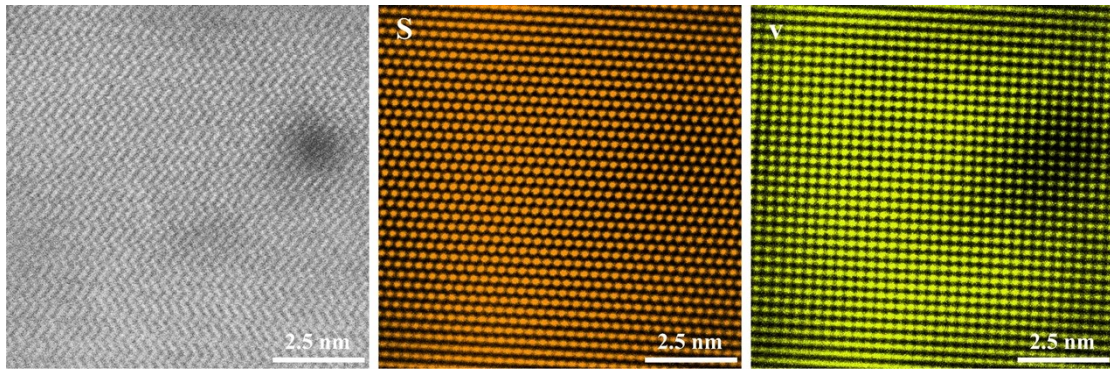


Fig. S6 AC-TEM images and atomic EDS mapping of the Rose D-VS₂.

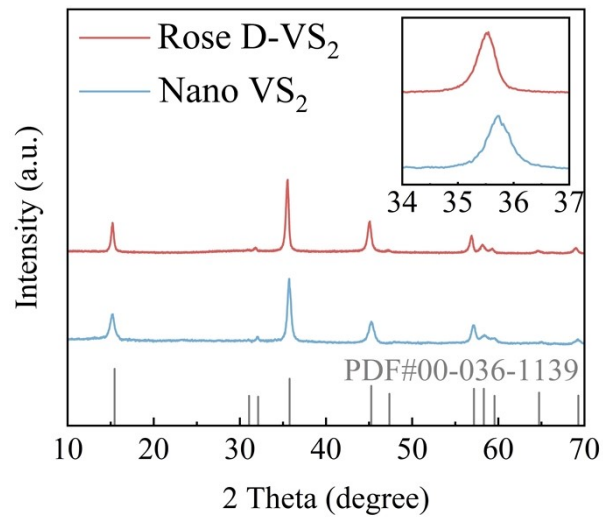


Fig. S7 XRD pattern of different VS₂ materials.

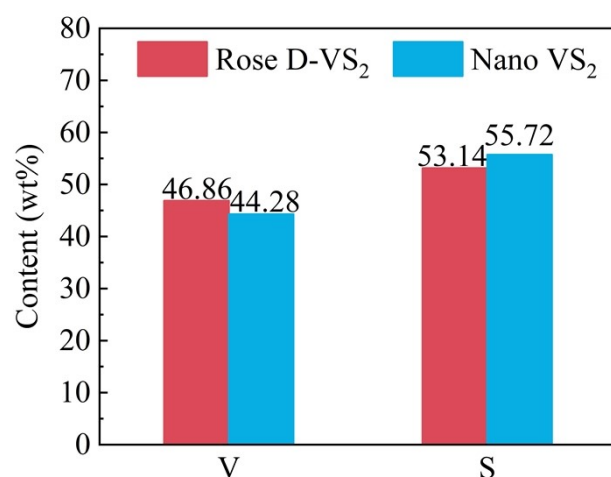


Fig. S8 Inductively coupled plasma (ICP) results showing the elemental ratios of different VS₂ materials.

The element ratio of V to S for the Nano VS₂ is 1:2, whereas the ratio for the Rose D-VS₂ is 5:9.

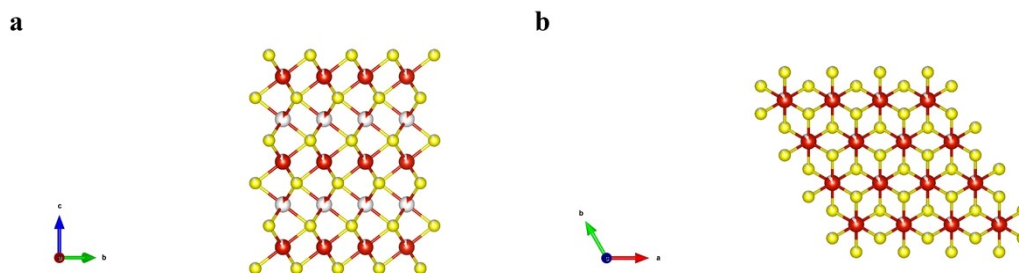


Fig. S9 The simulated atomic structure of the Rose D-VS₂.

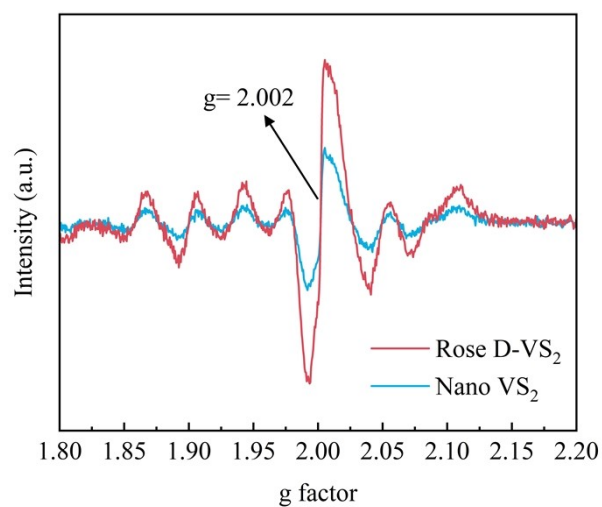


Fig. S10 Electron paramagnetic resonance (EPR) spectra of different VS_2 materials. The EPR spectra reveal abundant S vacancies ($g=2.002$) and vanadium in multiple oxidation states⁵⁻⁷ in the Rose D- VS_2 .

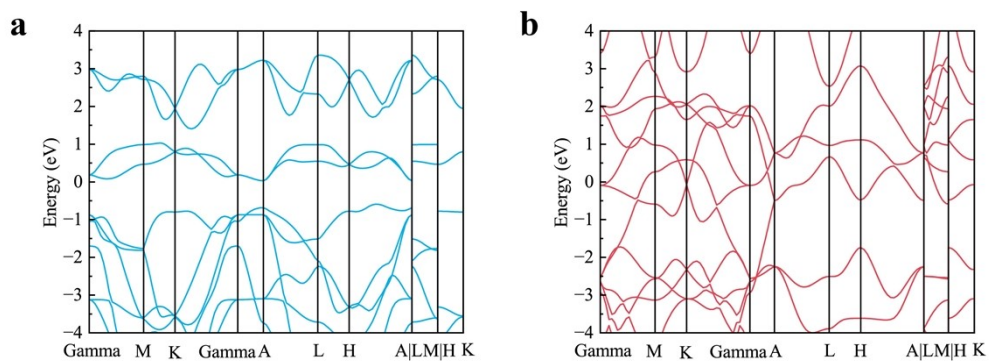


Fig. S11 The band-structure of a) the Nano VS_2 and b) the Rose D- VS_2 .

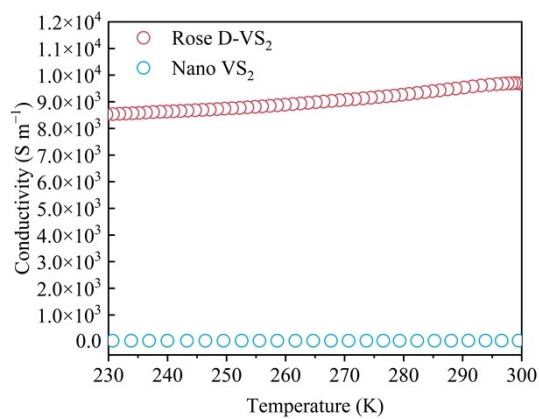


Fig. S12 Electric conductivity of different VS₂ materials.

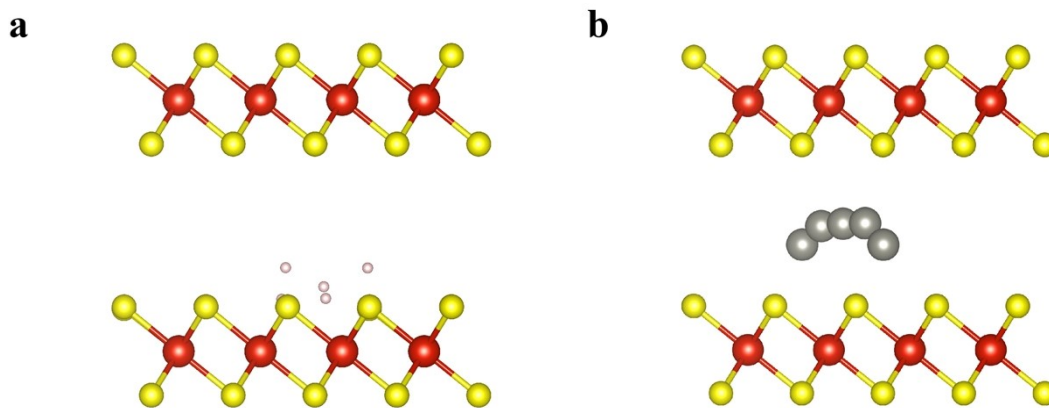


Fig. S13 The migration pathways of a) H⁺ ions and b) Zn²⁺ ions in the interlayer of the Nano VS₂.

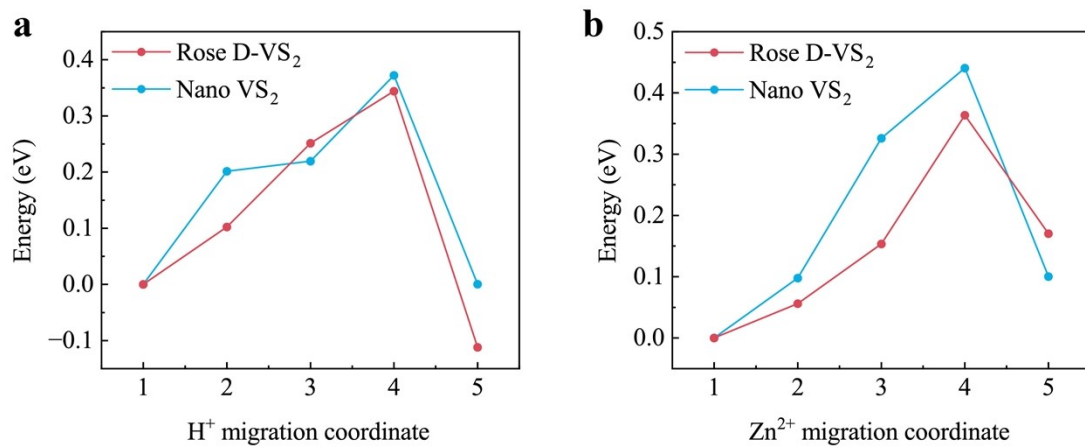


Fig. S14 The migration energy of a) H⁺ ions and b) Zn²⁺ ions in the interlayer of different VS₂ materials.

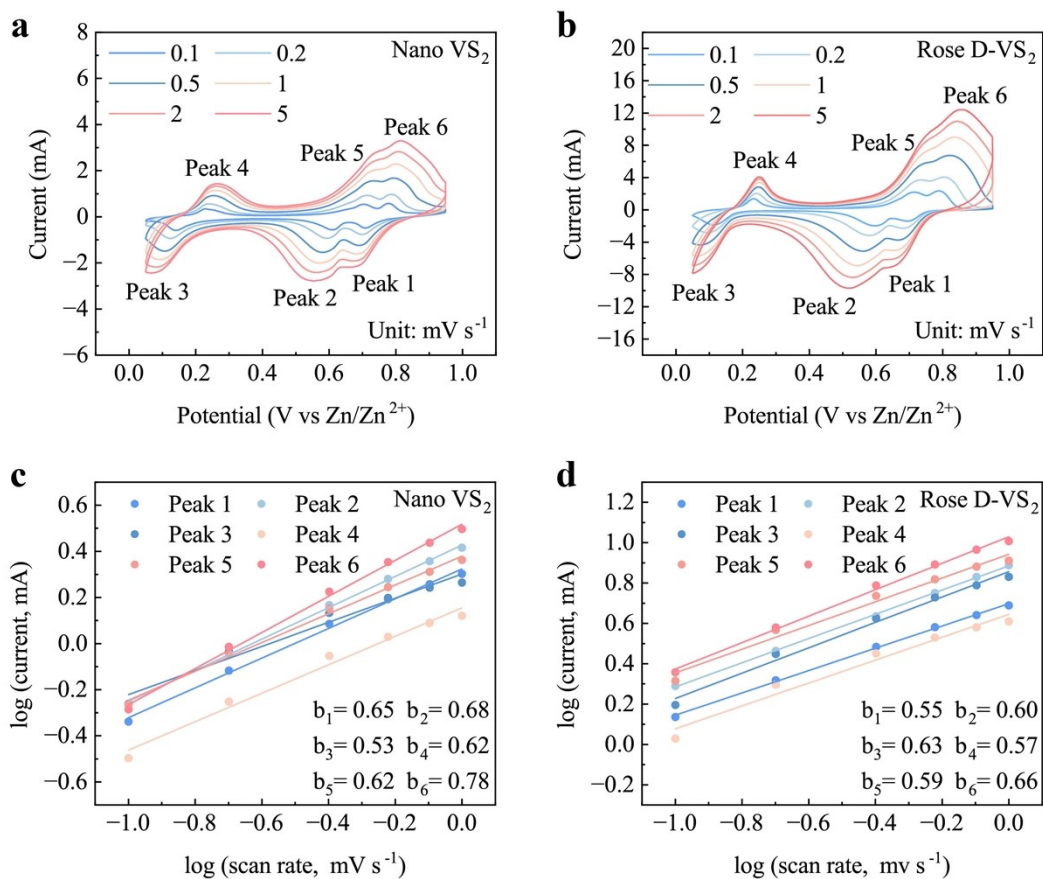


Fig. S15 Electrochemical reaction kinetics analysis of different VS₂ materials. a) CV profiles of the Nano VS₂ at various scan rates from 0.1 to 1.0 mV s⁻¹. b) CV profiles of the Rose D-VS₂ at various scan rates from 0.1 to 1.0 mV s⁻¹. c) Linear correlation between logarithm of peak current (i_p) and logarithm of scan rate (v) for the Nano VS₂. d) Linear correlation between logarithm of peak current (i_p) and logarithm of scan rate (v) for the Rose D-VS₂.

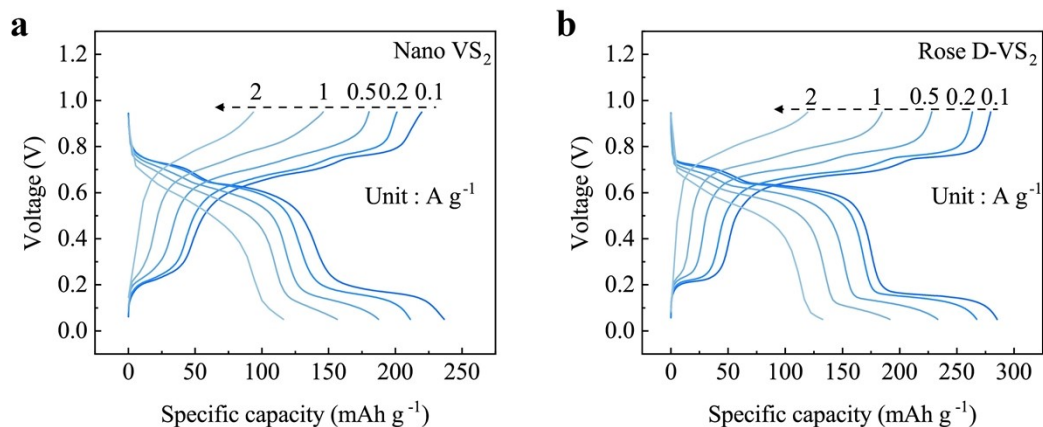


Fig. S16 Galvanostatic charge/discharge (GCD) curves for VS_2 cathodes at different currents.

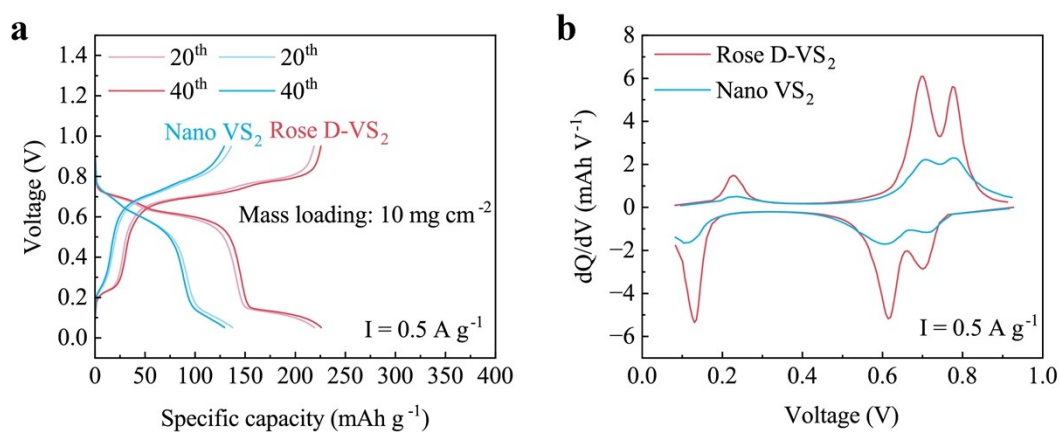


Fig. S17 Cycling performance of different VS_2 cathodes at 0.5 A g^{-1} . a) GCD curves for different VS_2 cathodes at 0.5 A g^{-1} . b) Differential capacity (dQ/dV) curves corresponding to the 20th cycle for different VS_2 cathodes.

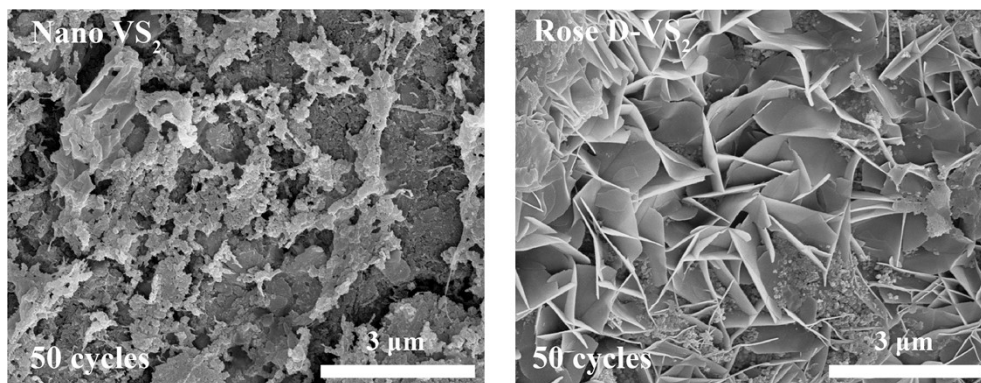


Fig. S18 SEM images showing the morphology of different VS₂ cathodes after 50 cycles at 0.5 A g⁻¹.

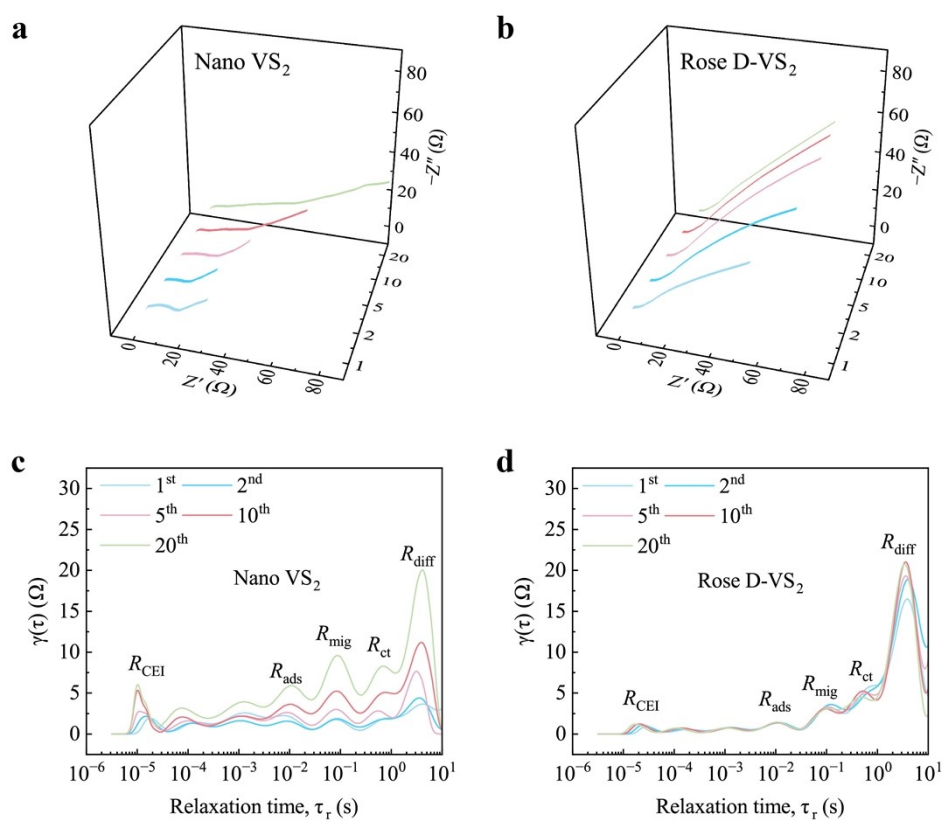


Fig. S19 a and b) EIS spectra of the Nano VS₂ cathode and the Rose D-VS₂ cathode with the mass loading of 10 mg cm⁻² at 0.5 A g⁻¹ after different cycles, respectively. c and d) Corresponding DRT curves of different VS₂ cathodes after different cycles.

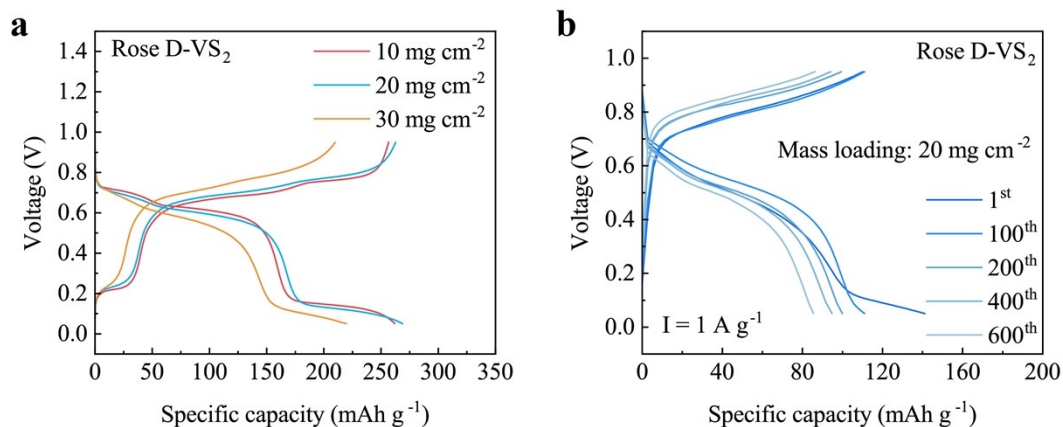


Fig. S20 GCD curves of the Rose D-VS₂ cathodes. a) GCD curves of the Rose D-VS₂ cathodes with different mass loading at 0.2 A g⁻¹. b) GCD curves of the Rose D-VS₂ cathodes with the mass loading of 20 mg cm⁻² at 1 A g⁻¹.

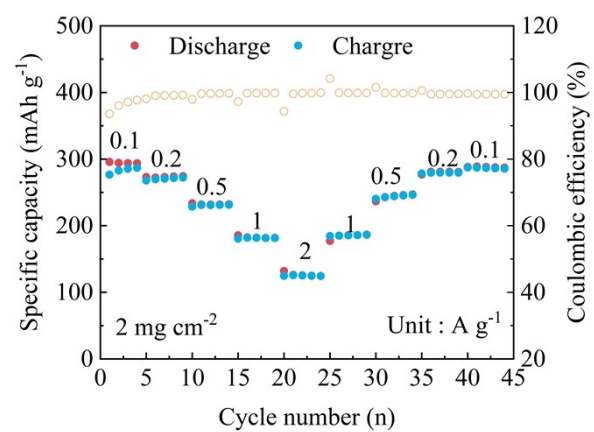


Fig. S21 The rate performance of the Rose D-VS₂ cathode with the mass loading of 2 mg cm⁻²

Table S1. Electrochemical performance of different VS₂ materials.

Material	Mass loading (mg cm⁻²)	Specific capacity (mAh g⁻¹)	Reference
VS ₂ nanoflowers	-	190.3 at 0.05 A g ⁻¹	S8
VS ₂ colloidal nanospheres	1.5-2	212.9 at 0.1 A g ⁻¹	S9
Hierarchical VS ₂ @SS	4-5	198 at 0.05 A g ⁻¹	S10
rGO-VS ₂ nanosheets	1	238 at 0.1 A g ⁻¹	S11
VS ₂ nanocrystal@N-C	1-2	203 at 0.05 A g ⁻¹	S12
VS ₂ @CF	5	261.5 at 0.2 A g ⁻¹	S13
VS ₂ Nanosheets	2	205.3 at 0.1 A g ⁻¹	S14
V-doped VS ₂ nanosheets	1.5	156.3 at 0.1 A g ⁻¹	S15
VS ₂ @Mxene	1	156.3 at 0.1 A g ⁻¹	S16
VS ₂ ⊥ V ₄ C ₃ T _x nanosheets	1-2	262.1 at 1 A g ⁻¹	S17
VS ₂ /Ti ₃ C ₂ T _z	1-2	285 at 0.2 A g ⁻¹	S18
VS ₂ microflowers	1-2.5	215.7 at 0.2 A g ⁻¹	S19
Our work	10	285 at 0.1 A g⁻¹ and 186 mAh g⁻¹ at 1 A g⁻¹	
	20	268.5 at 0.2 A g⁻¹	
	30	219.6 at 0.2 A g⁻¹	

Table S2. Air self-charging performance of different materials.

Material	Mass loading (mg cm⁻²)	Self-charging efficiency (%)	average self-charging rate (mAh g⁻¹ h⁻¹)	Reference
Poly(1,5-NAPD)	2	98.5	13.5	S20
NZnMn ₂ O _{4-x}	5.8	83.3	11.7	S21
CaZn _{0.36} VO	1	79.7	7.3	S22
VCF	1	60	7.5	S23
PTO	-	84.9	19.2	S24
PNZ-CMP	1-1.4	81.8	19.3	S25
COF	1-1.5	96.9	30	S26
BQPH	1.5	81.8	29	S27
Our work	10	105.9	53.7	

(1) self-charging efficiency
$$\eta = \frac{C_{self-charging}}{C_{galvanostatic}} \times 100\%$$

(2) average self-charging rate
$$\nu = \frac{C_{total-self-charging}}{t_{total}} \times 100\%$$

where $C_{self-charging}$, $C_{galvanostatic}$, and $C_{total-self-charging}$ denote self-charging discharge capacity, galvanostatic discharge capacity, and total discharge capacity after cyclic self-charging. t_{total} denotes the total cyclic self-charging time.

References

1. J. F. I. G. Kresse, *Physical Review B*, 1996, **54**, 11169.
2. D. J. G. Kresse, *Physical Review B*, 1999, **59**, 1758.
3. K. B. J.P. Perdew, M. Ernzerhof, *Physical Review Letter*, 1996, **77**, 3865-3868.
4. S. Grimme, J. Antony, S. Ehrlich and H. Krieg, *The Journal of Chemical Physics*, 2010, **132**.
5. Z. Li, Y. Ren, L. Mo, C. Liu, K. Hsu, Y. Ding, X. Zhang, X. Li, L. Hu, D. Ji and G. Cao, *ACS Nano*, 2020, **14**, 5581-5589.
6. C. J. Magon, J. F. Lima, J. P. Donoso, V. Lavayen, E. Benavente, D. Navas and G. Gonzalez, *Journal of Magnetic Resonance*, 2012, **222**, 26-33.
7. K. Zhu, S. Wei, H. Shou, F. Shen, S. Chen, P. Zhang, C. Wang, Y. Cao, X. Guo, M. Luo, H. Zhang, B. Ye, X. Wu, L. He and L. Song, *Nature Communications*, 2021, **12**, 6878.
8. P. He, M. Yan, G. Zhang, R. Sun, L. Chen, Q. An and L. Mai, *Advanced Energy Materials*, 2017, **7**, 1601920.
9. Y. Tan, S. Li, X. Zhao, Y. Wang, Q. Shen, X. Qu, Y. Liu and L. Jiao, *Advanced Energy Materials*, 2022, **12**, 2104001.
10. T. Jiao, Q. Yang, S. Wu, Z. Wang, D. Chen, D. Shen, B. Liu, J. Cheng, H. Li, L. Ma, C. Zhi and W. Zhang, *Journal of Materials Chemistry A*, 2019, **7**, 16330-16338.
11. T. Chen, X. Zhu, X. Chen, Q. Zhang, Y. Li, W. Peng, F. Zhang and X. Fan, *Journal of Power Sources*, 2020, **477**, 228652.
12. J. Liu, W. Peng, Y. Li, F. Zhang and X. Fan, *Journal of Materials Chemistry C*, 2021, **9**, 6308-6315.

13. Y. Mao, B. Zhao, J. Bai, H. Ma, P. Wang, W. Li, K. Xiao, S. Wang, X. Zhu and Y. Sun, *Small*, 2023, **19**, 2207998.
14. H. Sun, L. Yang, E. Hu, M. Feng, C. Fan, W. Wang, H. Li, X. Wang and Z. Liu, *ACS Applied Materials & Interfaces*, 2022, **14**, 40247-40256.
15. J. Gao, X. Qi, B. Yang, H. Quan, C. Hu, X.-F. Wang, C. Sun and S. Wang, *Journal of Alloys and Compounds*, 2023, **960**, 170550.
16. P. Meng, W. Wang, J. Shang, P. Liu, H. Xu, Q. Wang, S. Wang, F. Wang and X. Wang, *Small Methods*, 2023, **7**, 2201471.
17. Y. Mao, J. Bai, S. Lin, P. Wang, W. Li, K. Xiao, S. Wang, X. Zhu, B. Zhao and Y. Sun, *Small*, 2023, **20**, 2306615.
18. L. Zhang, Y. Li, X. Liu, R. Yang, J. Qiu, J. Xu, B. Lu, J. Rosen, L. Qin and J. Jiang, *Advanced Science*, 2024, **11**, 2401252.
19. T. Wang, W. Gao, Y. Zhao, S. Wang and W. Huang, *Journal of Materials Science & Technology*, 2024, **173**, 107-113.
20. L. Yan, Y. Zhang, Z. Ni, Y. Zhang, J. Xu, T. Kong, J. Huang, W. Li, J. Ma and Y. Wang, *Journal of the American Chemical Society*, 2021, **143**, 15369-15377.
21. W. Qiu, Z. Lin, H. Xiao, G. Zhang, H. Gao, H. Feng and X. Lu, *Materials Advances*, 2021, **2**, 6694-6702.
22. Y. Zhang, F. Wan, S. Huang, S. Wang, Z. Niu and J. Chen, *Nature Communications*, 2020, **11**, 2199.
23. M. Liao, J. Wang, L. Ye, H. Sun, P. Li, C. Wang, C. Tang, X. Cheng, B. Wang and H. Peng, *Journal of Materials Chemistry A*, 2021, **9**, 6811-6818.

24. F. Yue, Z. Tie, Y. Zhang, S. Bi, Y. Wang and Z. Niu, *Angewandte Chemie International Edition*, 2022, **61**, e202208513.
25. L. Zhong, J. Li, C. Liu, L. Fang, Z. Yuan, D. Yu and X. Chen, *Advanced Functional Materials*, 2023, **33**, 2215133.
26. L. Zhong, C. Wang, J. He, Z. lin, X. Yang, R. Li, S. Zhan, L. Zhao, D. Wu, H. Chen, Z. Tang, C. Zhi and H. Lv, *Advanced Materials*, 2024, **36**, 2314050.
27. Z. Tie, Y. Zhang, J. Zhu, S. Bi and Z. Niu, *Journal of the American Chemical Society*, 2022, **144**, 10301-10308.